1521-009X/45/12/1364–1371$25.00
DRUG METABOLISM AND DISPOSITION

https://doi.org/10.1124/dmd.117.078188
Drug Metab Dispos 45:1364–1371, December 2017

Expression and Functional Characterization of Breast Cancer-Associated Cytochrome P450 4Z1 in *Saccharomyces cerevisiae*

Matthew G. McDonald, Sutapa Ray, Clara J. Amorosi, Katherine A. Sitko, John P. Kowalski, Lorela Paco, Abhinav Nath, Byron Gallis, Rheem A. Totah, Maitreya J. Dunham, Douglas M. Fowler, and Allan E. Rettie

Departments of Medicinal Chemistry (M.G.M., S.R., J.P.K., L.P., A.N., B.G., R.A.T., A.E.R.), Genome Sciences (K.A.S., C.J.A., M.J.D., D.M.F.), and Bioengineering (D.M.F.), University of Washington, Seattle, Washington

Received August 19, 2017; accepted October 4, 2017

ABSTRACT

CYP4Z1 is an "orphan" cytochrome P450 (P450) enzyme that has provoked interest because of its hypothesized role in breast cancer through formation of the signaling molecule 20-hydroxyeicosatetraenoic acid (20-HETE). We expressed human CYP4Z1 in *Saccharomyces cerevisiae* and evaluated its catalytic capabilities toward arachidonic and lauric acids (AA and LA). Specific and sensitive mass spectrometry assays enabled discrimination of the regioselectivity of hydroxylation of these two fatty acids. CYP4Z1 generated 7-, 8-, 9-, 10-, and 11-hydroxy LA, whereas the 12-hydroxy metabolite was not detected. HET0016, the prototypic CYP4 inhibitor, only weakly inhibited laurate metabolite formation (IC_{50} ~15 μM). CYP4Z1 preferentially oxidized AA to the 14(S),15(R)-epoxide with high regioselectivity and stereoselectivity, a reaction that was also insensitive to HET0016, but neither 20-HETE nor 20-carboxy-AA were detectable metabolites. Docking of LA and AA into a CYP4Z1 homology model was consistent with this preference for internal fatty acid oxidation. Thus, human CYP4Z1 has an inhibitor profile and product regioselectivity distinct from most other CYP4 enzymes, consistent with CYP4Z1's lack of a covalently linked heme. These data suggest that, if CYP4Z1 modulates breast cancer progression, it does so by a mechanism other than direct production of 20-HETE.

Introduction

The CYP4 family in humans contains 12 genes and 13 transcribed enzyme products that typically oxidize fatty acids at their ω-termini (Hsu et al., 2007; Edson and Rettie, 2013). This substrate and product selectivity have been documented extensively for the CYP4A and CYP4F subfamilies (Johnston et al., 2011). Indeed, the metabolic conversion of arachidonic acid (AA) to the active signaling molecule, 20-hydroxyeicosatetraenoic acid (20-HETE), has physiologic relevance in a plethora of tissue types (Fan et al., 2015; Johnson et al., 2015). The importance of this metabolite has been elegantly demonstrated in transgenic mice, where increased formation of 20-HETE caused elevation in blood pressure that could be linked to the functional activities of CYP4A11 and CYP4F2 (Lai et al., 2012; Savas et al., 2016).

In contrast, much less is known about the substrate selectivity of other human CYP4 subfamily members, resulting in many being referred to as "orphan" cytochromes 450 (P450) (Stark and Guengerich, 2007; Kelly et al., 2011). Within the last 10 years, an important physiologic role has been established for CYP4F22 (Ohno et al., 2015), and significant progress has been made in better defining the catalytic activities of CYP4F11 (Tang et al., 2010; Edson et al., 2013), CYP4V2 (Nakano et al., 2009, 2012), and CYP4X1 (Stark et al., 2008).

CYP4Z1 is the least well characterized of the CYP4 enzymes. Originally, CYP4Z1 was identified in breast tissue and noted to be upregulated in breast carcinoma (Rieger et al., 2004). In a more recent study, MCF-7 breast cancer cells exhibited aberrant CYP4Z1 protein targeted to the cell surface, and anti-CYP4Z1 autoantibodies were observed in sera of breast cancer patients, but not in that of controls (Nunna et al., 2017). CYP4Z1 expression has also been proposed as a biomarker for the existence of malignancy and/or progression of ovarian and prostate cancer (Downie et al., 2005; Tradonsky et al., 2012). Notably, stable overexpression of CYP4Z1 in breast cancer cells has been reported to promote angiogenesis and tumor growth in mice with a concomitant increase in cellular 20-HETE (Yu et al., 2012). The foregoing studies prompt the hypothesis that CYP4Z1 may act as a prognostic biomarker through generation of 20-HETE in cancer cells; however, many oxidized metabolites of AA can act as signaling molecules, and a full evaluation of the metabolite profile generated from AA by CYP4Z1 has not been previously performed.

This work was supported, in part, by Grants [R24GM115277] and [RO1GM109743] from the National Institutes of Health. MJD is supported in part by a Faculty Scholars grant from the Howard Hughes Medical Institute. MJD is also a senior fellow in the Genetic Networks program at the Canadian Institute for Advanced Research.

http://doi.org/10.1124/dmd.117.078188.

This article has supplemental material available at dmd.aspetjournals.org.

ABBREVIATIONS: AA, arachidonic acid; $APCI^-$, atmospheric pressure–negative chemical ionization; BHT, butylated hydroxytoluene; CO, carbon monoxide; CPR, cytochrome P450 oxido-reductase; DHET, dihydroxyeicosatrienoic acid; EET, epoxyeicosatrienoic acid; ESI^-, negative electrospray ionization; GC-MS, gas chromatography-mass spectrometry; HETE, hydroxyeicosatetraenoic acid; LA, lauric acid; LC-MS/MS, liquid chromatography-tandem mass spectrometry; MRM, multiple-reaction monitoring; 15-OH-PDA, 15-hydroxypentadecanoic acid; P450, cytochrome P450; PFB, pentafluorobenzyl ester.

Here, we report the first analysis of AA metabolism by recombinant CYP4Z1 expressed in *Saccharomyces cerevisiae*. CYP4Z1 forms no detectable oxidized metabolites at the ω-terminus, but instead it epoxidizes AA at the 14,15-double bond with high regioselectivity and stereoselectivity. In addition, CYP4Z1 is relatively insensitive to inhibition by the prototypic CYP4 inhibitor, HET0016. If CYP4Z1 has a role to play in modulating cancer progression, these new data suggest that the mechanism does not involve direct 20-HETE generation by this enzyme.

Materials and Methods

General Reagents

18-HETE, 19-HETE, 20-HETE, 20-HETE-d_6, 14,15- epoxyeicosatrienoic acid (14,15-EET), and 14,15-EET-d_{11} chemical standards were purchased from Cayman Chemical (Ann Arbor, MI). The 9-, 10-, 11-, and 12-hydroxy LA standards were previously synthesized (Guan et al., 1998). Recombinant CYP2C19 and CYP4F2 supersomes, coexpressed in insect cells with cytochrome P450 oxido-reductase (CPR) and cytochrome b5, were procured from Corning Inc. (Corning, NY). The CPR and cytochrome b5 used in CYP4Z1 incubations were expressed and purified according to established protocols (Chen et al., 1998). Organic solvents were obtained from Fisher Scientific (Pittsburgh, PA), and all other chemicals (including LA, AA, NADPH, BSTFA, 15-OH PDA, etc.) were purchased from Sigma-Aldrich (St. Louis, MO).

Cloning and Vector Construction

The p41KGAL1 vector was derived from the p416GAL1 vector (Mumberg et al., 1995) and the pUG6 vector (Guldener et al., 1996) using polymerase chain reaction and Gibson assembly to clone the KanMX cassette into p416GAL1 (Supplemental Table 1: primers KAS381, KAS382, KAS378, KAS379). To construct the p41KGAL1_CYP4Z1-HA vector, the *S. cerevisiae* codon-optimized CYP4Z1 sequence (Uniprot: Q86W10) with a C-terminal HA tag (Integrated DNA Technologies) was directionally cloned into the p41KGAL1 vector using SpeI-HF and SalI-HF (New England Biosciences, Ipswich, MA). Ligated plasmids were transformed into F' competent *Escherichia. coli* and verified by Sanger sequencing (Supplemental Fig. 1: plasmid sequences).

Expression of CYP4Z1 in Yeast

The yeast strain YMD3289 (S288C MATα HAP1+ ura3Δ0 leu2Δ1 his3Δ1 trp1Δ63) was transformed with p41KGAL1_CYP4Z1-HA. When required, yeast media were supplemented with 200 μg/ml G418 to maintain the plasmid. Unless otherwise specified, all cultures were grown at 28°C. To induce P450 expression, a single yeast colony was inoculated into 30 ml SC+-Ade medium (synthetic complete, 2% glucose, 30 mg/liter additional adenine) with G418 and grown at 30°C overnight. A 1:100 dilution of the overnight culture was inoculated into 500 ml of YPGE medium (10 g/liter yeast extract, 20 g/liter peptone, 5 g/liter glucose, 3% ethanol) with G418 and grown for 24 hours, at which point 2% galactose (w/v) was added to induce P450 expression. Cells were grown for an additional 15 hours, pelleted by centrifugation for 10 minutes at 4000*g*, and then frozen at −80°C for microsome preparation.

Western Blotting

One microgram of microsomes from control yeast or from yeast-expressing recombinant human CYP4Z1 was separated on a 4 - 12% Bis-Tris SDS-PAGE (Invitrogen, Carlsbad, CA) and transferred electrophoretically to nitrocellulose. After blocking for 2.5 hours with 5% w/v bovine serum serum, 5% w/v nonfat dry milk in phosphate-buffered salime, and 0.1% Triton X-100, the nitroceullose was reacted overnight with a 1:2000 dilution of rabbit anti-human CYP4Z1 primary antibody (Sigma Atlas, Darmstadt, Germany), followed by incubation with a 1: 10,000 dilution of anti-rabbit IgG, HRP-linked antibody (Cell Signaling Technology, Danvers, MA).

Preparation of Yeast Microsomes

Yeast microsomes were prepared as described previously (Pompon et al., 1996) using the enzymatic breaking procedure and PEG-4000/NaCl method with modifications to buffer volumes. Harvested cells (~3 g of wet weight) were washed with 15 ml of TEK buffer (50 mM Tris-HCl, pH 7.4, 1 mM EDTA, 0.1 M KCl), resuspended in 15 ml of TEM buffer (50 mM Tris-HCl, pH 7.4, 1 mM EDTA, 70 mM 2-mercaptoethanol), and incubated at room temperature for 5–10 minutes. Cells were recovered and resuspended in 1.5 ml of TMS buffer (1.5 M sorbitol; 20 mM Tris-MES, pH 6.3; 2 mM EDTA), and 5 mg of 20T Zymolyase was added. Cells were incubated for 1 hour at 28°C. Further steps were performed on ice. Spheroplasts were pelleted at 6732*g* and washed with 15 ml of TES-A buffer (50 mM Tris-HCl, pH 7.4, 1 mM EDTA, 1.5 M sorbitol), and the centrifugation step was repeated. Spheroplasts were resuspended in 10 ml of TES-B buffer (50 mM Tris-HCl, pH 7.4; 1 mM EDTA; 0.6 M sorbitol) and lysed using a Braun Labsonic U sonicator at a relative output power of 0.25 with 0.9 duty period using 2 × 15-second pulses. After 5 minutes on ice, lysed cells were centrifuged for 4 minutes at 1700*g*, and the supernatant was centrifuged for 10 minutes at 10,700*g* to remove the mitochondria. The supernatant volume was measured and TES-B buffer was added to 30 ml of total volume. Eight microliters of 50% PEG 4000 was added dropwise to this mixture, followed by 2 ml of 2.5 M NaCl, and the mixture was incubated on ice for 15 minutes. The mixture was then centrifuged for 10 minutes at 10,700*g*. The microsomal pellet was resuspended in 2 ml of TEG buffer (50 mM Tris-HCl pH 7.4, 1 mM EDTA, 20% (v/v) glycerol) and frozen at −80°C.

CYP4Z1 Quantitation by Carbon Monoxide Binding UV-Visible Spectroscopy

Carbon monoxide (CO) binding spectra by reduced CYP4Z1 were recorded on an Olis modernized Aminco DW-2 spectrophotometer (Olis, Bogart, GA). CYP4Z1 yeast microsomes were diluted 2-fold in 50 mM KPi buffer, pH 7.4, containing 20% glycerol, 1 mM EDTA, and 0.2% EMULGEN. Sodium dithionite (excess, powder) and methyl viologen (1.2 μM) were added, and the microsomes were then split equally between sample and reference quartz cuvettes before taking a baseline scan from 400 to 500 nm, at 25°C. CO gas was bubbled to saturation through the sample cuvette microsomes, and difference scans were taken of the CO-bound enzyme. Holo-CYP4Z1 concentrations were calculated according to Beer's law, taking the absorbance difference between the peak maximum (at ~450 nm) and the baseline (at 490 nm) and using an extinction coefficient of 91 $mM^{-1}cm^{-1}$ (Liu and Franklin, 1985).

General Microsomal Incubation Procedures

AA Assay. CYP4Z1 yeast microsomes (5–15 pmol/reaction), CPR, and cytochrome b5 (in a 1:2:1 molar ratio) were added to 100 mM potassium phosphate buffer, pH 7.4, and incubated on ice for 30 minutes. Sodium pyruvate (1 mM final concentration), HET0016 (1 μM, added only for inhibition reactions), and AA (75 μM) were successively added, and reactions were preincubated at 37°C/75 rpm in a water bath for 3 minutes before initiation through the addition of NADPH (1 mM in a 200-μl final reaction volume). A high AA substrate concentration was chosen to ensure better saturation and facilitate identification of the full complement of metabolites without kinetic concerns. After 15 minutes' incubation, reactions were quenched with 1 ml of ethyl acetate containing 0.01% butylated hydroxytoluene (BHT), and 100 ng each of 20-HETE-d_6 and 14,15-EET-d_{11} were added as internal standards. Reaction mixtures were vortexed, centrifuged, and the organic layer collected; then the extraction process was repeated with another 1 ml of ethyl acetate/BHT. The combined organic layers were evaporated at room temperature under a nitrogen gas stream, and the residue reconstituted in 10 μl of dimethylsulfoxide, with another 40 μl of a 50:50 solution of a 4:1 mix of acetonitrile/methanol in water subsequently added, for LC-MS analysis. Incubations and workup were all carried out in the dark, and all organic solvents (including those used to make up substrate and standard stock solutions, which were stored at −80°C) were degassed before use. Methanol, from the AA and HET0016 stock solutions, did not exceed 1% of the final reaction volume. Reactions with P450 supersomes (Corning Inc.) contained 15 pmol of P450 enzyme, 1 mM sodium pyruvate, 75 μM AA, and 1 mM NADPH in 200 μl of 100 mM potassium phosphate buffer, pH 7.4. Incubation and workup conditions were identical to those described here for CYP4Z1. Calibration curves were prepared by spiking variable amounts of 18-HETE (for CYP4F12 metabolic analysis) or 19-HETE and 14,15-EET into 200 μl of potassium phosphate buffer containing 1 mM sodium pyruvate, to generate standard mixtures with final concentrations of between 2.5 and 500 pg/μl

buffer. These standard solutions, prepared in duplicate, were immediately worked up and analyzed in an identical fashion to that described in the preceding for the incubation samples .

LA Assay. CYP4Z1 yeast microsomes (5–15 pmol per reaction), CPR, and cytochrome b5 (in a 1:2:1 molar ratio) were reconstituted in 100 mM potassium phosphate buffer, pH 7.4, and incubated on ice for 30 minutes, after which LA was added (1 mM final concentration). Reactions were preincubated for 3 minutes at 37°C/75 rpm in a water bath before initiation through the addition of NADPH (1 mM in a 500-μl final reaction volume). After 30 minutes' incubation, reactions were quenched with 50 μl of 10% HCl, 10 nmol of 15-OH PDA was added as internal standard, and the solutions were extracted twice with 900 μl of ethyl acetate. The organic solvent was evaporated under a nitrogen stream, and the residues were dissolved in 50 μl of ethyl acetate. BSTFA reagent (Sigma), 50 μl, was added, and the silylation reactions were heated to 90°C for 60 minutes. After cooling, the samples were analyzed by gas chromatography-mass spectrometry (GC-MS). Calibration curves were prepared by spiking concentrated standard mixtures containing variable amounts of 9, 10, 11, and 12-hydroxy LAs, into 500 μl of potassium phosphate buffer (final concentrations, 0.005–25 μM). The standard buffer solutions, prepared in duplicate, were worked up and analyzed in identical fashion to the incubation reactions described herein.

Analysis of LA Metabolites by GC-MS

GC-MS analyses were performed on a Shimadzu QP2010 Gas Chromatograph Quadrupole mass spectrometer (Shimadzu Scientific, Columbia, MD) using electron impact (EI) ionization. The various hydroxylated LA metabolites, as well as the internal standard, 15-OH PDA, were analyzed as their respective *bis*-trimethylsilylated derivatives by selected ion monitoring (SIM) of the following mass channels: *m/z* 345 (12-OH LA), *m/z* 173 (7-OH LA), *m/z* 159 (8-OH LA), *m/z* 145 (9-OH LA), *m/z* 131 (10-OH LA), *m/z* 117 (11-OH LA), and *m/z* 387 (15-OH PDA). The derivatized metabolites were separated on a Restek Rxi-5Sil MS (fused silica), 30 m, 0.25-μm GC column with 0.25-mm internal diameter at an injection temperature of 250°C. The method used an initial column temperature of 80°C, which was held for 0.5 minute, and then increased to 160°C at a rate of 30°C/min. From there, the rate was slowed to 5°C/min up to a temperature of 225°C and was subsequently increased to 40°C/min until reaching a final temperature of 290°C. The 9, 10, 11, and 12-hydroxy LA metabolites were quantified by comparing peak area ratios (relative to the internal standard, 15-OH PDA) to ratios from the appropriate calibration curve, determined with previously synthesized hydroxy LA standards (Guan et al., 1998), using linear regression analysis. Since standards of the 7- and 8-hydroxy LAs were unavailable, rates of LA metabolism to these compounds were estimated using the 9-hydroxy LA calibration curve.

Analysis of AA Metabolites by LC-MS/MS

LC-MS/MS analyses were conducted on a Waters Xevo TQ-S Tandem Quadrupole mass spectrometer (Waters Co., Milford, MA) coupled to an ACQUITY Ultra-Performance LC (UPLC) System with integral autoinjector (Waters). The Xevo was operated in ESI^--MS/MS (multiple-reaction monitoring, MRM) mode at a source temperature of 150°C and a desolvation temperature of 200°C. The following mass transitions were monitored in separate ion channels for the various oxidative AA metabolites/standards: *m/z* 337 > 145 (5,6-dihydroxyeicosatrienoic acid, DHET), *m/z* 337 > 127 (8,9-DHET), *m/z* 337 > 167 (11,12-DHET), *m/z* 337 > 207 (14,15-DHET), *m/z* 334 > 289 (20-COOH-AA), *m/z* 330 > 219 (14,15-EET-d_{11}), *m/z* 325 > 281 (20-HETE-d_6), *m/z* 319 > 115 (5-HETE), *m/z* 319 > 155 (8-HETE and 8,9-EET), *m/z* 319 > 151 (9-HETE), *m/z* 319 > 167 (11-HETE and 11,12-EET), *m/z* 319 > 179 (12-HETE and 11,12-EET), *m/z* 319 > 191 (5,6-EET), *m/z* 319 > 208 (12-HETE and 11,12-EET), *m/z* 319 > 219 (15-HETE and 14,15-EET), *m/z* 319 > 245 (20-HETE), *m/z* 319 > 247 (17-HETE), *m/z* 319 > 261 (18-HETE) and *m/z* 319 > 275 (19-HETE). The cone voltage was set to 20 V for all compounds and optimized collision energies were set to 16 eV for 20-COOH-AA, 17-HETE, 18-HETE, 19-HETE, 20-HETE, and 20-HETE-d_6, 10 eV for all other HETEs, as well as for all of the EETs, and 15 eV for all DHETs. Note: 17-HETE and 18-HETE metabolite formation was monitored only for CYP4F12 supersomes (Supplemental Fig. 2).

Metabolic products from the AA incubations were separated on an Acquity BEH Shield C_{18}, 1.7 μ, 2.1 × 100 mm, UPLC column (Waters Corp) using a binary solvent gradient, solvent A (0.05% aqueous acetic acid), and solvent B (4:1 acetonitrile/methanol plus 0.05% acetic acid, with a constant flow rate of 0.3 ml/min). From 0 to 5.5 minutes, the method was isocratic at 55% B and then increased to 58% B over 0.5 minute. The concentration was maintained at 58% B for another 12 minutes. Metabolites were quantified through comparison of their peak area ratios (relative to the 20-HETE-d_6 or 14,15-EET-d_{11} internal standard peak areas) to calibration curves using linear regression analysis. Limits of detection for 19-HETE, 20-HETE, and 14,15-EET were below 50 fmol injected on column.

Inhibition of Fatty Acid Metabolism by HET0016

CYP4Z1 (5 pmol), CPR, and cytochrome b5 were incubated in potassium phosphate buffer on ice for 30 minutes, as described. LA (100 μM final concentration) and HET0016 (variable concentration, 0–500 μM) were then added from 200 × concentrated methanolic stock solutions. Reactions were incubated and worked up as previously described for the LA assay. Duplicate incubations were carried out at each inhibitor concentration.

Alternatively, CYP4F12 supersomes (15 pmol) were incubated with AA (75 μM), sodium pyruvate (1 mM), and NADPH (1 mM) in 200 μl of potassium phosphate buffer for 15 minutes, as described already for the AA assay, with the addition of HET0016 in the incubation mixtures (at variable concentrations, 0–500 μM). Again, reactions were incubated and worked up as previously described, and duplicate incubations were carried out at each inhibitor concentration (Supplemental Fig. 3).

Preparation of 14,15-EET-Pentafluorobenzyl Ester Derivatives

AA metabolites were converted to their pentafluorobenzyl ester derivatives according to the procedure of Mesaros et al. (2010). AA, at 5 μM, was incubated with either CYP4Z1 yeast microsomes or CYP2C19 supersomes as described above. 14,15-EET-d_{11} (50 ng) was added as internal standard, and the incubations were extracted with ethyl acetate/BHT and evaporated under nitrogen. The evaporated residue was reconstituted in 100 μl of dichloromethane (DCM), and 100 μl of a 1:19 solution of diisopropylethyl amine in DCM, followed by 100 μl of a 1:9 mixture of pentafluorobenzyl bromide in DCM, was subsequently added. The reactions were allowed to shake, in the dark, at room temperature for 30 minutes; then solvent was removed under a nitrogen stream. Residues were resolubilized in 300 μl of a 97:3 hexane/ethanol solution for LC-MS/MS analysis.

Chiral Resolution and Electron Capture APCI-MS of 14,15-EET-PFB Esters

LC-MS/MS analyses of the derivatized EET-PFB esters were conducted on the Waters Xevo TQ-S MS/ACQUITY UPLC system (Waters) described herein. The Xevo was operated in $APCI^-$-MS/MS (MRM) mode at a source temperature of 150°C and a probe temperature of 500°C. The following mass transitions were monitored: *m/z* 330 > 219 (14,15-EET-d_{11}), *m/z* 319 > 219 (14,15-EET) with a cone voltage of 40 V and a collision energy of 10 eV set for both channels (under APCI conditions, EET-PFB esters undergo in-source loss of PFB to (re)generate the 14,15-EET anion). The 14,15-EET-PFB enantiomers were resolved on a Chiralpak AD 2.1 × 250 mm, 10 μ column (Daicel Chemical Industries, Ltd., West Chester, PA) at a flow rate of 0.7 ml/min using an isocratic solvent gradient of 98.5% hexane (solvent A) and 1.5% hexane/IPA (4:6, solvent B) as described (Mesaros et al., 2010).

Homology Modeling of CYP4Z1 and Ligand Docking

A homology model for CYP4Z1 was constructed using the I-TASSER server (Yang et al., 2015), with no templates or experimental constraints specified. The primary template identified by I-TASSER was the CYP4B1 structure (PDB ID: 5T6Q), along with other P450 crystal structures (PDB IDs: 1TQN, 3MDM, and 4J14).

Ligand docking was performed in AutoDock Vina (Trott and Olson, 2010). The hydrogen bond weight was doubled to better model the interactions between the carboxylate of the ligands and basic/hydrogen bonding amino acids in the active site, according to a previously described protocol for P450 ligand docking (Hsu et al., 2017). Models of AA and LA were generated in Open Babel (O'Boyle et al., 2011) at pH 7.4 with Gasteiger charges added, and ligand and protein files were processed using AutoDock tools. The side chains of active-site residues Leu117, Val126, Val379, Asn381, and Ser383 were set to be flexible, whereas

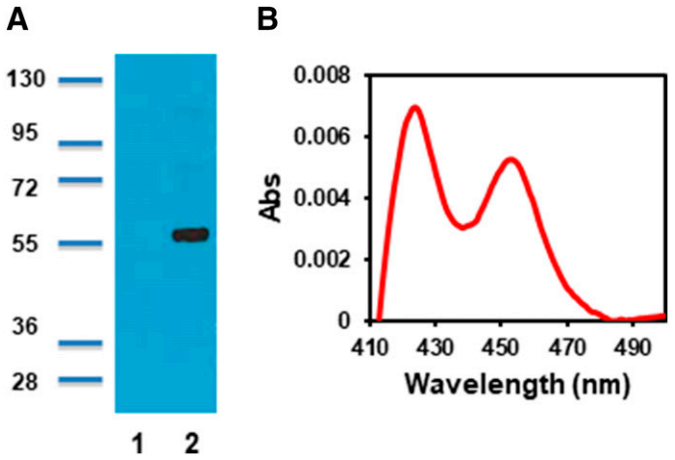

Fig. 1. Characterization of CYP4Z1 expressed in yeast microsomes. (A) Western blot of microsomes harvested from untransformed yeast (lane 1) and from yeast expressing CYP4Z1 (lane 2). (B) Carbon monoxide difference spectrum of reduced CYP4Z1 microsomes.

backbone atoms and all other remaining residues (and heme) of the homology model were held rigid. Visualization of the docked ligands in the active site was performed in Chimera (Pettersen et al., 2004).

Homology model coordinates have been deposited in the Protein Model Database (https://bioinformatics.cineca.it/PMDB/) with ID PM0081238.

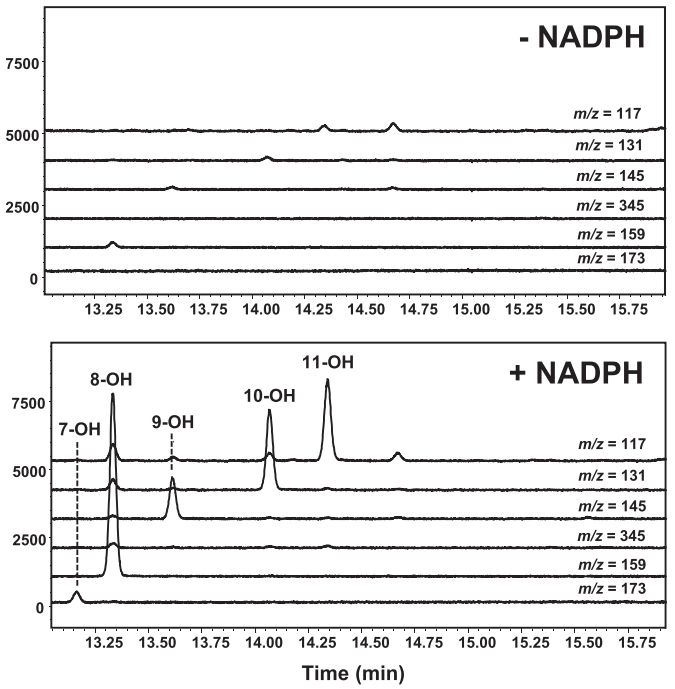

Fig. 2. GC-MS chromatogram of LA metabolites generated by recombinant CYP4Z1. The chromatograms show resolution of the hydroxylated products generated from incubations of LA with CYP4Z1-expressing yeast microsomes in the presence (bottom traces) and absence (top traces) of NADPH cofactor (LA metabolites were quantitatively converted to their (bis)trimethylsilyl derivatives before analysis). Individual metabolites were identified by selected ion monitoring (SIM) of the optimal, differentiating mass fragmentation ions for each derivatized regioisomer (7-OH LA, *m/z* = 173; 8-OH LA, *m/z* = 159; 9-OH LA, *m/z* = 145; 10-OH LA, *m/z* = 131; 11-OH LA, *m/z* = 117 and 12-OH LA, *m/z* = 345). 12-OH LA (Rt = 15.6 minutes) concentrations were below the limit of detection (i.e., <0.02 pmol were produced/min per picomoles CYP4Z1).

TABLE 1

Rates of LA and AA metabolite formation by CYP4Z1 microsomes

Substrate[a]	Metabolite	Rate (pmol/pmol per minute)
LA	7-OH LA	~2[b]
LA	8-OH LA	~40[b]
LA	9-OH LA	6.1 ± 0.7
LA	10-OH LA	16.0 ± 1.4
LA	11-OH LA	8.8 ± 0.2
LA	12-OH LA	n.d.
AA	19-HETE	0.048 ± 0.004
AA	20-HETE	n.d.
AA	20-COOH-AA	n.d.
AA	14,15-EET	1.9 ± 0.06

n.d., not detected.
[a]Substrate concentrations: 1 mM LA; 75 μM AA.
[b]Since we lacked synthetic standards for the 7- and 8-hydroxy metabolites of LA, these values were estimated using the 9-OH LA calibration curve.

Data Analysis

Quantitative incubation experiments for measurement of LA and AA CYP4Z1 metabolites were performed with three replicate samples on two different preparations of yeast microsomes. As a result of enzyme constraints imposed by low CYP4Z1 expression levels, the HET0016 IC_{50} values for inhibition of LA metabolism were determined in a single experiment using duplicate data points. All other experiments, unless otherwise indicated, were performed with three replicate samples. Data presented are means ± S.D. unless otherwise stated. IC_{50} values were determined in GraphPad Prism version 7.00 (GraphPad Software, La Jolla, CA) using the one-site fit log(inhibitor) versus response (three parameters) model.

Results

Characterization of CYP4Z1 Expressed in Yeast. CYP4Z1 expression in microsomes prepared from *S. cerevisiae* was evaluated by SDS-PAGE followed by Western blot analysis using a CYP4Z1 polyclonal peptide antibody. The blot identified a single band at approximately 58 kDa (Fig. 1A) in yeast microsomes, which displayed a typical P450 difference spectrum (Fig. 1B) after reduction with dithionite and saturation with carbon monoxide. The specific content of CYP4Z1 ranged from 10 to 20 pmol/mg protein across multiple

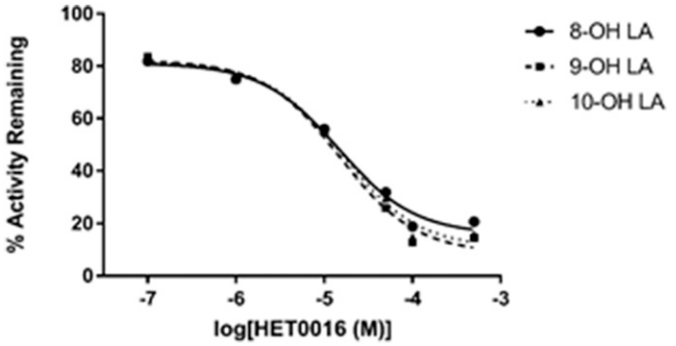

Fig. 3. HET0016 inhibition of CYP4Z1-catalyzed LA metabolism. The overlaid graphs show the relative IC_{50} curves for inhibition of yeast microsomal CYP4Z1-mediated LA 8-, 9-, and 10-hydroxylase activity by HET0016, a low nanomolar inhibitor of most CYP4 enzymes. Data points denote the mean turnover rate of LA to each metabolite, obtained from duplicate incubations of 100 μM LA and HET0016 (at concentrations ranging from 0.1 to 500 μM) with CYP4Z1 microsomes, expressed as a percentage of the rate obtained in the absence of inhibitor. HET0016 inhibited formation of 8-OH LA, 9-OH LA, and 10-OH LA with IC_{50} values of 14.7, 14.9, and 15.9 μM, respectively (we were unable to generate reasonable IC_{50} curves in this experiment for either 7-OH LA, owing to low turnover rates, or 11-OH LA, owing to overlap of the derivatized metabolite peak with HET0016).

expression attempts. The exact position of the Soret band could not be determined because of the relatively high ratio of cytochrome c oxidase to CYP4Z1 in these microsomal preparations, which dominated the Soret region of CO binding spectra of microsomes prepared from empty vector controls (data not shown).

Metabolism of Lauric Acid by CYP4Z1. First, we evaluated CYP4Z1-dependent metabolism of LA because medium-chain saturated fatty acids are the only substrates for the enzyme to have been examined, albeit in whole yeast cells (Zollner et al., 2009). CYP4Z1-expressing yeast microsomes incubated with LA and NADPH generated five internal alcohol metabolites but none of the terminal 12-hydroxy metabolite (Fig. 2). Alcohols were analyzed by GC-MS as their trimethylsilyl derivatives, which permitted unambiguous assignment of the biologically generated 7-OH, 8-OH, 9-OH, 10-OH, and 11-OH metabolites from their characteristic fragmentations. Formation of midchain LA alcohols by CYP4Z1 was expected because the 7-OH, 8-OH, 9-OH, and 10-OH metabolites are also generated by CYP4Z1-expressing *Schizosaccharomyces pombe* cells (Zollner et al., 2009); however, our findings expand the CYP4Z1 metabolite profile to include 11-OH LA, generated by CYP4Z1-expressing yeast microsomes. The 7-OH, 8-OH, 9-OH, 10-OH, and 11-OH LAs were formed in a ratio of ~1:20:3:8:4 (Table 1). Although HET0016 is a nanomolar inhibitor of most CYP4 enzymes, it inhibited CYP4Z1-mediated LA 8-, 9-, and10-hydroxylation relatively weakly with an average IC_{50} of 15 μM (Fig. 3).

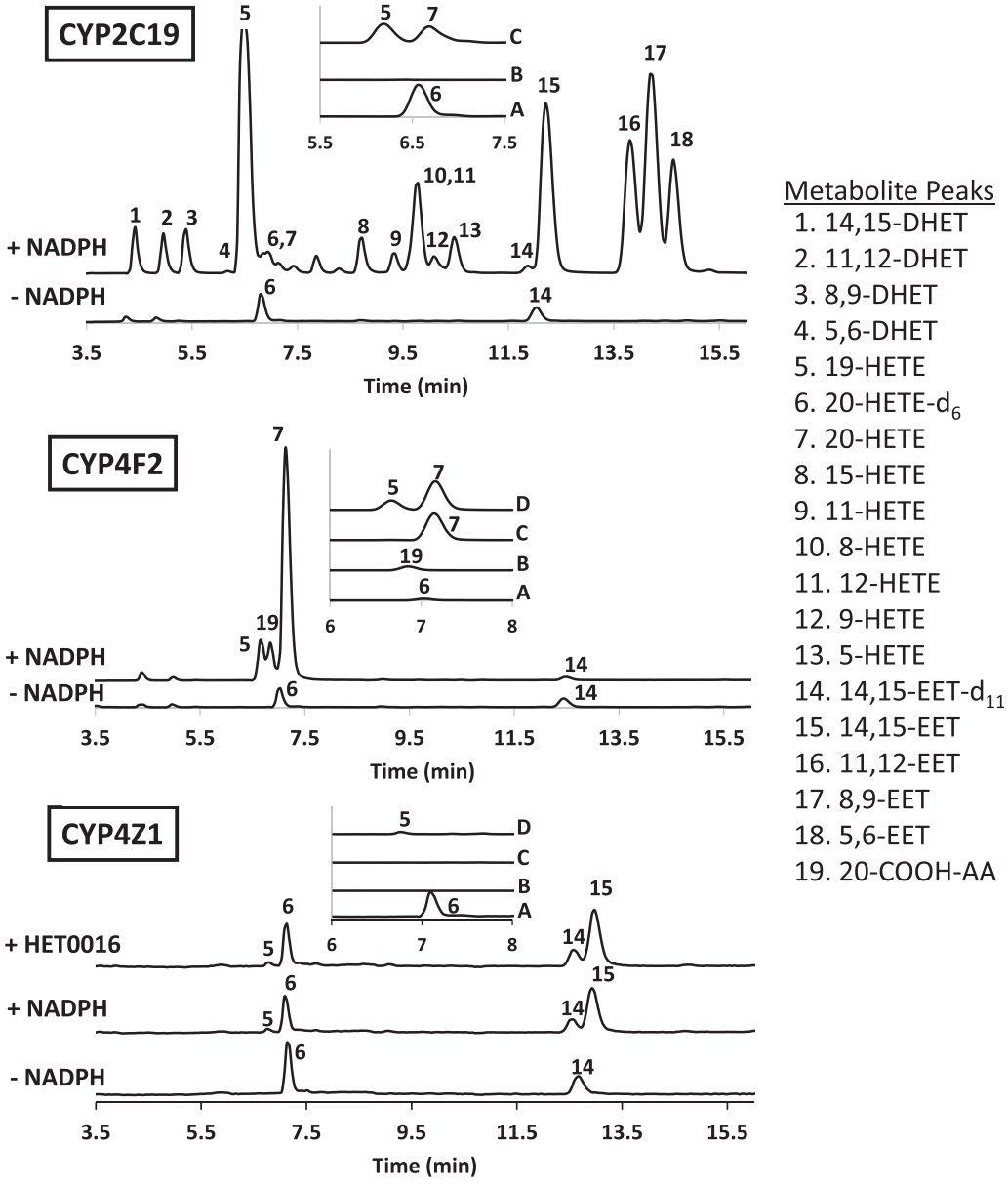

Fig. 4. ESI^- LC-MS/MS chromatograms of AA metabolism by cytochrome P450s. Total ion chromatograms (TICs) of metabolites produced from incubations of 75 μM AA with CYP2C19 and CYP4F2 Supersomes and with CYP4Z1 yeast microsomes, in the presence and absence of NADPH (TICs = sum of 17 individual AA metabolite MRM channels plus channels for the internal standards, 20-HETE-d_6 and 14,15-EET-d_{11}). An additional TIC is included to show (the lack of) HET0016 inhibition of CYP4Z1 AA metabolism at 1 μM HET0016. Insets represent magnifications of individual MRM chromatograms from the (+) NADPH incubations of P450 with AA (peaks are normalized to the same scale): (A) m/z = 325 > 281 (20-HETE-d_6), (B) m/z = 333 > 271 (20-COOH-AA), (C) m/z = 319 > 245 (20-HETE), and (D) m/z = 319 > 275 (19-HETE).

Metabolism of AA by CYP4Z1. P450 enzymes can transform AA into a plethora of metabolites, as exemplified by the diversity of regioisomeric EETs and HETEs generated by CYP2C19 (Fig. 4, upper panel). In contrast, NADPH-supplemented CYP4Z1 microsomes formed only (cis) 14,15-EET and a trace amount of 19-HETE (Fig. 4, lower panel; Table 1). CYP4Z1 formed no detectable 20-HETE or 20-carboxy AA metabolites, despite the fact that these are prominent metabolites of CYP4F2 (Fig. 4, middle panel). Similar to metabolism of LA, HET0016 was not an effective inhibitor of CYP4Z1-catalyzed AA metabolism, showing no inhibition at the commonly used concentration of 1 μM (Fig. 4, lower panel). Finally, we evaluated the stereochemistry of the major 14,15-EET metabolite generated by CYP4Z1. Chiral-phase analysis demonstrated that CYP4Z1 generated the *cis*-14(S),15(R)-EET with 80% enantiomeric excess (Fig. 5). Stereochemistry was assigned based on the relative elution of 14,15-EET enantiomers produced by CYP2C19, as reported previously (Mesaros et al., 2010).

Homology Modeling of CYP4Z1 and Ligand Docking. The homology model for CYP4Z1 shows an active site containing the hydrophobic amino acid residues Leu117, Val126, and Val379 that help confine aliphatic regions of fatty acid substrates. Toward the "mouth" of this substrate-binding pocket are the hydrogen-bonding residues Asn381 and Ser383 (Fig. 6, A and B). The highest-affinity lauric acid (LA) pose is situated with the ω-1,2,3,4 positions all close to the heme iron, with measured distances of 5.0, 4.7, 3.7, and 4.7 Å. These correspond to the 11-, 10-, 9-, and 8-OH products, respectively. The highest-affinity pose that was generated for AA is positioned for 14,15-EET production, with carbons 14 and 15 situated 4.9 and 6.1 Å, respectively, from the heme iron (Fig. 6B). The carboxylate moieties of AA and LA are located 2.4 and 1.9 Å, respectively, from Asn381, suggesting that hydrogen-bonding interactions with this amino acid may serve to position the internal aliphatic sections of the substrates over the heme for oxidation. Although Ser383 is located, respectively, 4.7 and 6.4 Å away from the LA and AA carboxylate moieties in these models, other slightly lower-affinity configurations place the residue within hydrogen-bonding distance of the acid groups (data not shown), suggesting that Ser383 might also play a role in positioning the fatty acids within the CYP4Z1 active site. Given the limitations of homology modeling and computational docking, these poses should not be regarded as atomically precise. Instead, they represent plausible models of CYP4Z1/substrate complexes that are fully consistent with our experimental data.

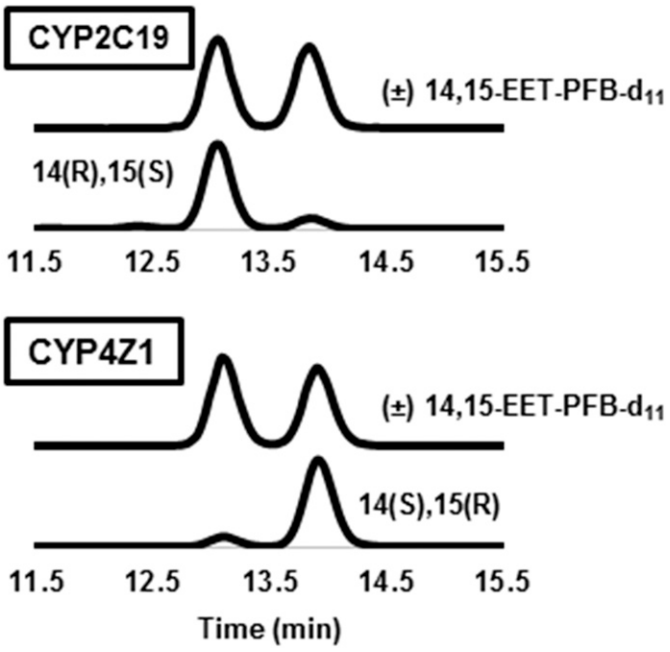

Fig. 5. LC-MS/MS chromatograms showing stereoselective formation of 14,15-EET by CYP4Z1 and CYP2C19. The chromatograms show chiral resolution of the 14,15-EET metabolic products isolated from incubations of AA with either CYP4Z1 yeast microsomes or CYP2C19 supersomes (with (±)14,15-EET-d_{11} added as internal standard). Metabolites and standards were derivatized to their PFB esters and then analyzed by electron-capture APCI$^-$ LC-MS/MS (resolution was achieved on a Chiralpak AD column).

Discussion

Before our work, the only data available regarding catalysis by CYP4Z1 were obtained from expression of the enzyme in *S. pombe*, followed by whole-cell biotransformation studies with LA and myristic acid (Zollner et al., 2009) and in microsomes from T47D cells that had been transfected with CYP4Z1 (Yu et al., 2012). The former efforts identified *internal* monohydroxylated fatty acid metabolites rather than formation of the expected ω-hydroxy products by CYP4Z1. The microsomal studies reported here, with budding yeast-expressed CYP4Z1, confirm the formation of several mid-chain alcohols from LA and extend the metabolite profile to include 11-OH LA. This somewhat unusual profile for a CYP4 enzyme is, nonetheless, in line with expectations based on the absence of a heme covalent link in CYP4Z1 (Table 2). The covalent link cannot exist in this enzyme because CYP4Z1 lacks the I-helix glutamic acid residue that forges an ester bond with the heme (LeBrun et al., 2002; Zheng et al., 2003). Instead, CYP4Z1 has an alanine at this position (Table 2). The reported substrate selectivity of CYP4F8, CYP4F12, and CYP4X1 supports this theory as each of these enzymes also lacks the I-helix glutamate residue and has likewise been shown to prefer internal rather than ω-fatty acid oxidation of AA (Table 2),

Given the preceding structural argument, 20-HETE generation by CYP4Z1, as reported by Yu et al. (2012), seemed unusual; so we examined the full metabolite profile of AA by LC-MS/MS. These studies revealed 14,15-EET to be the major metabolite, with no evidence for 20-HETE production. Cognizant of the differences between the two studies, we went to extreme lengths to ensure that we were not overlooking, or misassigning, a 20-HETE pathway in CYP4Z1-expressing yeast microsomes. First, we developed a recombinant expression system that provided demonstrably active CYP4Z1 (via the generated CO-difference spectrum) in the microsomal preparations used for the metabolic studies. Second, we confirmed that our microsomal enzyme preparations recapitulated the internal hydroxylations of LA that were expected based on 1) an earlier study in whole yeast cells (Zollner et al., 2009), and 2) the structural features of the enzyme. Third, we developed a highly sensitive and highly specific LC-MS/MS assay for 20-HETE that had a limit of detection of 50 fmol on column, equivalent to a turnover rate of ~5 pmol/min per nanomole of CYP4Z1. Therefore, if CYP4Z1 generated 20-HETE in any significant amount, we would have observed it. Additionally, since we found earlier that CYP4F2 could sequentially metabolize vitamin K to a terminal acid metabolite (Edson et al., 2013), we considered the possibility that CYP4Z1 might convert 20-HETE to 20-carboxy-AA. LC-MS/MS analysis did not support this scenario, however, despite an appropriate enzyme control (CYP4F2). A final control of the AA metabolite profile generated by CYP4F12, which also lacks a heme covalent link, was reinvestigated. As expected, we found that this enzyme generated 18-HETE instead of 20-HETE as the major hydroxylated metabolite (Supplemental Fig. 2), further validating our analytical procedures. In the aggregate, our studies provide convincing evidence *against* ω-hydroxylation of fatty acids by CYP4Z1, in line with the evolving structure-function relationships for

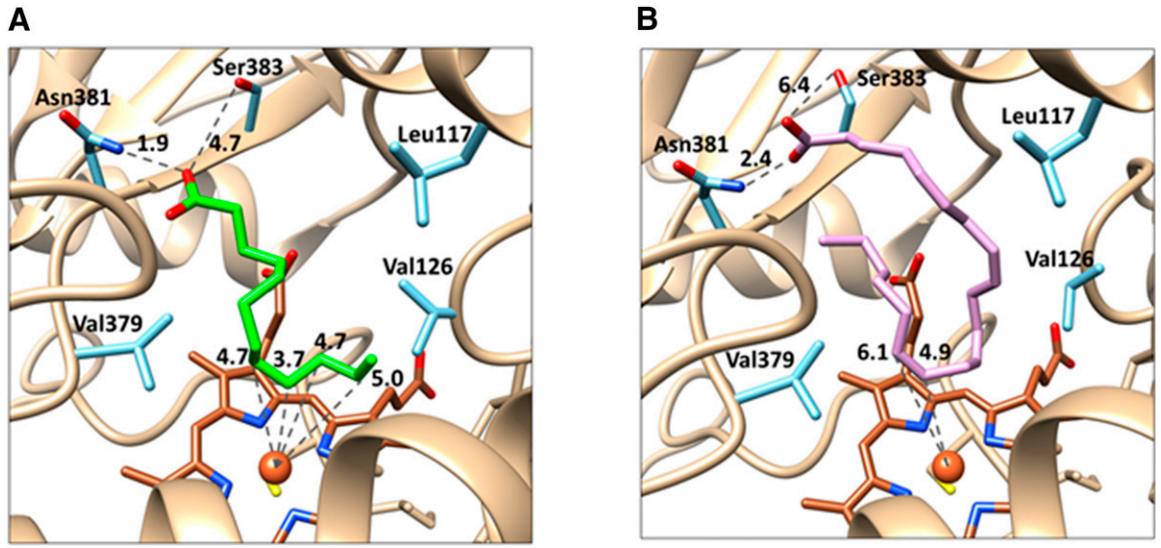

Fig. 6. 3D Homology models of the CYP4Z1 active site with LA and AA docked. The CYP4Z1 amino acid residues shown in light blue are believed to be of primary importance to substrate binding, with Leu117, Val126, and Val379 forming a hydrophobic pocket encapsulating the fatty chains of LA (green, A) and AA (lavender, B). Asn381 appears to anchor both substrates in the active site, likely through electrostatic interactions formed between the Asn amine and the fatty acid carboxylate moieties (~2 Å distant). (A) The model of LA bound to CYP4Z1 shows internal carbons of the fatty acid centered over the heme (brown), with C-8 through C-11 of LA all located between 3.7 and 5.0 Å from the heme iron atom. By contrast, the terminal carbon of LA is oriented away from the heme iron at 6.3 Å. (B) The model of AA bound to CYP4Z1 likewise shows the terminal carbon of the fatty acid to be pointed away from the heme, whereas the C_{14}-C_{15} double bond of AA is only 5 to 6 Å distant from the heme iron. In the figure, oxygen atoms are shown in red, nitrogen atoms in dark blue, sulfur atoms in yellow, and the heme iron as a brown sphere.

CYP4 enzymes that cannot forge a covalent heme link. Reasons for the differences between the two studies are unknown at this time, but they might reflect the varied cell systems and/or analytical procedures employed. Additional studies with purified reconstituted CYP4Z1 are needed to define fully the enzyme's substrate and product specificities.

Interestingly, CYP4Z1 also demonstrates relatively modest inhibition by the prototypic CYP4 inhibitor, HET0016. CYP4 enzymes that are committed ω-hydroxylases typically exhibit IC_{50} values for this formamidoxime inhibitor less than 100 nM (Parkinson et al., 2012; Edson and Rettie, 2013); however, HET0016 inhibited LA hydroxylation catalyzed by CYP4Z1 with an IC_{50} of only 15 μM. Presumably, the structural features that promote ω-hydroxylation by most CYP4 enzymes (Hsu et al., 2017) also impart tighter binding and inhibition by HET0016. We attempted to test this hypothesis by looking at HET0016 inhibition of AA metabolism by CYP4F12 Supersomes, the only commercially available CYP4 enzyme lacking the I-helix glutamate residue that enables formation of the covalent heme link. We were able to confirm literature reports that CYP4F12 primarily metabolizes AA to 18-HETE with little to no 20-HETE formation (Stark et al., 2005), although we did also observe the production of 17-HETE and 19-HETE as minor metabolites (Supplemental Fig. 2). HET0016 inhibited CYP4F12-mediated AA metabolism with an IC_{50} of ~600 nM (Supplemental Fig. 3). Although this value is significantly lower than observed for HET0016 inhibition of CYP4Z1-mediated LA metabolism, it is still ~10-fold higher than literature values reported for HET0016 inhibition of more typical CYP4 ω-hydroxylase enzymes. More extensive studies with other CYP4 enzymes lacking the heme covalent link are needed to confirm this apparent cosegregation.

Whereas both 20-HETE production and CYP4 enzyme expression are increased in a number of human cancers (Alexanian et al., 2012), our findings are suggestive of a role for 14,15-EET in these malignant events, in accord with several literature reports (Jiang et al., 2007; Mitra et al., 2011; Wei et al., 2014). Indeed, a specific role for racemic 14,15-EET, formed by CYP3A4 and acting to mediate breast cancer cell growth through Stat3, has been advanced (Mitra et al., 2011). In preliminary studies, we have confirmed that CYP3A4 forms 14,15-EET

TABLE 2

Relationship between the presence of a predicted heme covalent link and 20-HETE formation in human CYP4 enzymes

Subfamily	Enzyme	Localization	Covalent Heme	AA Metabolite
CYP4A	4A11	Liver, kidney	Yes (FEGHDT)	20-HETE Powell et al. (1998)
	4A22	Liver, kidney	Yes (FEGHDT)	—
CYP4FB	4B1	Lung, bladder	Yes (FEGHDT)	—
CYP4V	4V2	Retina	Yes (FEGHDT)	20-HETE Nakano (2011)
CYP4F	4F2	Liver, kidney	Yes (FEGHDT)	20-HETE Powell et al. (1998)
	4F3A	Myeloid tissues	Yes (FEGHDT)	20-HETE Fer et al. (2008)
	4F3B	Liver, kidney	Yes (FEGHDT)	20-HETE Christmas et al. (2001)
	4F11	Liver, kidney	Yes (FEGHDT)	20-HETE Tang et al. (2010)
	4F22	Skin	Yes (FEGHDT)	—
	4F8	Urogenital	No (FGGHDT)	18-HETE Bylund et al. (2000)
	4F12	Liver, intestine	No (FGGHDT)	18-HETE Bylund et al. (2001)
CYP4X	4X1	Brain, skin	No (LAGHDT)	14,15-EET Stark et al. (2008)
CYP4Z	4Z1	Breast tissue	No (FAGHDT)	20-HETE Yu et al. (2012)
	4Z1	Breast tissue	No (FAGHDT)	14,15-EET (current study)

with little stereochemical bias (data not shown). Therefore, since CYP4Z1 formed 14(S),15(R)-EET with high stereoselectivity, it will be interesting to contrast the effects of the two epoxide enantiomers on breast cancer cell growth and invasiveness. Finally, our data provide a cautionary note about the use of HET0016 as a pan-CYP4 inhibitor, particularly at low micromolar concentrations in cellular studies to diagnose involvement of CYP4 enzymes that do not possess a covalently modified heme.

Authorship Contributions

Participated in research design: Fowler, Dunham, McDonald, Rettie.

Conducted experiments: McDonald, Amorosi, Ray, Sitko.

Contributed new reagents or analysis tools: Totah, Gallis, Kowalski, Paço, Nath.

Performed data analysis: McDonald, Ray, Rettie.

Wrote or contributed to the writing of the manuscript: McDonald, Fowler, Rettie.

References

Alexanian A, Miller B, Roman RJ, and Sorokin A (2012) 20-HETE-producing enzymes are up-regulated in human cancers. *Cancer Genomics Proteomics* **9**:163–169.

Bylund J, Bylund M, and Oliw EH (2001) cDna cloning and expression of CYP4F12, a novel human cytochrome P450. *Biochem Biophys Res Commun* **280**:892–897.

Bylund J, Hidestrand M, Ingelman-Sundberg M, and Oliw EH (2000) Identification of CYP4F8 in human seminal vesicles as a prominent 19-hydroxylase of prostaglandin endoperoxides. *J Biol Chem* **275**:21844–21849.

Chen W, Koenigs LL, Thompson SJ, Peter RM, Rettie AE, Trager WF, and Nelson SD (1998) Oxidation of acetaminophen to its toxic quinone imine and nontoxic catechol metabolites by baculovirus-expressed and purified human cytochromes P450 2E1 and 2A6. *Chem Res Toxicol* **11**:295–301.

Christmas P, Jones JP, Patten CJ, Rock DA, Zheng Y, Cheng SM, Weber BM, Carlesso N, Scadden DT, Rettie AE, et al. (2001) Alternative splicing determines the function of CYP4F3 by switching substrate specificity. *J Biol Chem* **276**:38166–38172.

Downie D, McFadyen MC, Rooney PH, Cruickshank ME, Parkin DE, Miller ID, Telfer C, Melvin WT, and Murray GI (2005) Profiling cytochrome P450 expression in ovarian cancer: identification of prognostic markers. *Clin Cancer Res* **11**:7369–7375.

Edson KZ, Prasad B, Unadkat JD, Suhara Y, Okano T, Guengerich FP, and Rettie AE (2013) Cytochrome P450-dependent catabolism of vitamin K: ω-hydroxylation catalyzed by human CYP4F2 and CYP4F11. *Biochemistry* **52**:8276–8285.

Edson KZ and Rettie AE (2013) CYP4 enzymes as potential drug targets: focus on enzyme multiplicity, inducers and inhibitors, and therapeutic modulation of 20-hydroxyeicosatetraenoic acid (20-HETE) synthase and fatty acid ω-hydroxylase activities. *Curr Top Med Chem* **13**: 1429–1440.

Fan F, Muroya Y, and Roman RJ (2015) Cytochrome P450 eicosanoids in hypertension and renal disease. *Curr Opin Nephrol Hypertens* **24**:37–46.

Fer M, Corcos L, Dréano Y, Plée-Gautier E, Salaün JP, Berthou F, and Amet Y (2008) Cytochromes P450 from family 4 are the main omega hydroxylating enzymes in humans: CYP4F3B is the prominent player in PUFA metabolism. *J Lipid Res* **49**:2379–2389.

Guan X, Fisher MB, Lang DH, Zheng YM, Koop DR, and Rettie AE (1998) Cytochrome P450-dependent desaturation of lauric acid: isoform selectivity and mechanism of formation of 11-dodecenoic acid. *Chem Biol Interact* **110**:103–121.

Güldener U, Heck S, Fielder T, Beinhauer J, and Hegemann JH (1996) A new efficient gene disruption cassette for repeated use in budding yeast. *Nucleic Acids Res* **24**:2519–2524.

Hsu MH, Baer BR, Rettie AE, and Johnson EF (2017) The crystal structure of cytochrome P450 4B1 (CYP4B1) monooxygenase complexed with octane discloses several structural adaptations for ω-hydroxylation. *J Biol Chem* **292**:5610–5621.

Hsu MH, Savas U, Griffin KJ, and Johnson EF (2007) Human cytochrome p450 family 4 enzymes: function, genetic variation and regulation. *Drug Metab Rev* **39**:515–538.

Jiang JG, Ning YG, Chen C, Ma D, Liu ZJ, Yang S, Zhou J, Xiao X, Zhang XA, Edin ML, et al. (2007) Cytochrome p450 epoxygenase promotes human cancer metastasis. *Cancer Res* **67**: 6665–6674.

Johnson AL, Edson KZ, Totah RA, and Rettie AE (2015) Cytochrome P450 ω-hydroxylases in inflammation and cancer. *Adv Pharmacol* **74**:223–262.

Johnston JB, Ouellet H, Podust LM, and Ortiz de Montellano PR (2011) Structural control of cytochrome P450-catalyzed ω-hydroxylation. *Arch Biochem Biophys* **507**:86–94.

Kelly EJ, Nakano M, Rohatgi P, Yarov-Yarovoy V, and Rettie AE (2011) Finding homes for orphan cytochrome P450s: CYP4V2 and CYP4F22 in disease states. *Mol Interv* **11**:124–132.

Lai G, Liu X, Wu J, Liu H, and Zhao Y (2012) Evaluation of CMV and KAP promoters for driving the expression of human CYP4F2 in transgenic mice. *Int J Mol Med* **29**:107–112.

LeBrun LA, Xu F, Kroetz DL, and Ortiz de Montellano PR (2002) Covalent attachment of the heme prosthetic group in the CYP4F cytochrome P450 family. *Biochemistry* **41**:5931–5937.

Liu Z and Franklin MR (1985) Cytochrome P-450 ligands: metyrapone revisited. *Arch Biochem Biophys* **241**:397–402.

Mesaros C, Lee SH, and Blair IA (2010) Analysis of epoxyeicosatrienoic acids by chiral liquid chromatography/electron capture atmospheric pressure chemical ionization mass spectrometry using [13C]-analog internal standards. *Rapid Commun Mass Spectrom* **24**:3237–3247.

Mitra R, Guo Z, Milani M, Mesaros C, Rodriguez M, Nguyen J, Luo X, Clarke D, Lamba J, Schuetz E, et al. (2011) CYP3A4 mediates growth of estrogen receptor-positive breast cancer cells in part by inducing nuclear translocation of phospho-Stat3 through biosynthesis of (±)-14,15-epoxyeicosatrienoic acid (EET). *J Biol Chem* **286**:17543–17559.

Mumberg D, Müller R, and Funk M (1995) Yeast vectors for the controlled expression of heterologous proteins in different genetic backgrounds. *Gene* **156**:119–122.

Nakano M (2011) *Biochemical characterization of CYP4V2 and its role in the retinal disease, in* Biettie Crystalline Dystrophy. University of Washington, Seattle.

Nakano M, Kelly EJ, and Rettie AE (2009) Expression and characterization of CYP4V2 as a fatty acid omega-hydroxylase. *Drug Metab Dispos* **37**:2119–2122.

Nakano M, Kelly EJ, Wiek C, Hanenberg H, and Rettie AE (2012) CYP4V2 in Bietti's crystalline dystrophy: ocular localization, metabolism of ω-3-polyunsaturated fatty acids, and functional deficit of the p.H331P variant. *Mol Pharmacol* **82**:679–686.

Nunna V, Jalal N, and Bureik M (2017) Anti-CYP4Z1 autoantibodies detected in breast cancer patients. *Cell Mol Immunol* **14**:572–574.

O'Boyle NM, Banck M, James CA, Morley C, Vandermeersch T, and Hutchison GR (2011) Open babel: an open chemical toolbox. *J Cheminform* **3**:33.

Ohno Y, Nakamichi S, Ohkuni A, Kamiyama N, Naoe A, Tsujimura H, Yokose U, Sugiura K, Ishikawa J, Akiyama M, et al. (2015) Essential role of the cytochrome P450 CYP4F22 in the production of acylceramide, the key lipid for skin permeability barrier formation. *Proc Natl Acad Sci USA* **112**:7707–7712.

Parkinson OT, Kelly EJ, Bezabih E, Whittington D, and Rettie AE (2012) Bioactivation of 4-Ipomeanol by a CYP4B enzyme in bovine lung and inhibition by HET0016. *J Vet Pharmacol Ther* **35**:402–405.

Pettersen EF, Goddard TD, Huang CC, Couch GS, Greenblatt DM, Meng EC, and Ferrin TE (2004) UCSF Chimera–a visualization system for exploratory research and analysis. *J Comput Chem* **25**:1605–1612.

Pompon D, Louerat B, Bronine A, and Urban P (1996) Yeast expression of animal and plant P450s in optimized redox environments. *Methods Enzymol* **272**:51–64.

Powell PK, Wolf I, Jin R, and Lasker JM (1998) Metabolism of arachidonic acid to 20-hydroxy-5,8,11, 14-eicosatetraenoic acid by P450 enzymes in human liver: involvement of CYP4F2 and CYP4A11. *J Pharmacol Exp Ther* **285**:1327–1336.

Rieger MA, Ebner R, Bell DR, Kiessling A, Rohayem J, Schmitz M, Temme A, Rieber EP, and Weigle B (2004) Identification of a novel mammary-restricted cytochrome P450, CYP4Z1, with overexpression in breast carcinoma. *Cancer Res* **64**:2357–2364.

Savas Ü, Wei S, Hsu MH, Falck JR, Guengerich FP, Capdevila JH, and Johnson EF (2016) 20-Hydroxyeicosatetraenoic acid (HETE)-dependent hypertension in human cytochrome P450 (CYP) 4A11 transgenic mice: normalization of blood pressure by sodium restriction, hydrochlorothiazide, or blockade of the type 1 angiotensin ii receptor. *J Biol Chem* **291**:16904–16919.

Stark K, Dostalek M, and Guengerich FP (2008) Expression and purification of orphan cytochrome P450 4X1 and oxidation of anandamide. *FEBS J* **275**:3706–3717.

Stark K and Guengerich FP (2007) Characterization of orphan human cytochromes P450. *Drug Metab Rev* **39**:627–637.

Stark K, Wongsud B, Burman R, and Oliw EH (2005) Oxygenation of polyunsaturated long chain fatty acids by recombinant CYP4F8 and CYP4F12 and catalytic importance of Tyr-125 and Gly-328 of CYP4F8. *Arch Biochem Biophys* **441**:174–181.

Tang Z, Salamanca-Pinzón SG, Wu ZL, Xiao Y, and Guengerich FP (2010) Human cytochrome P450 4F11: heterologous expression in bacteria, purification, and characterization of catalytic function. *Arch Biochem Biophys* **494**:86–93.

Tradonsky A, Rubin T, Beck R, Ring B, Seitz R, and Mair S (2012) A search for reliable molecular markers of prognosis in prostate cancer: a study of 240 cases. *Am J Clin Pathol* **137**:918–930.

Trott O and Olson AJ (2010) AutoDock Vina: improving the speed and accuracy of docking with a new scoring function, efficient optimization, and multithreading. *J Comput Chem* **31**:455–461.

Wei X, Zhang D, Dou X, Niu N, Huang W, Bai J, and Zhang G (2014) Elevated 14,15- epoxyeicosatrienoic acid by increasing of cytochrome P450 2C8, 2C9 and 2J2 and decreasing of soluble epoxide hydrolase associated with aggressiveness of human breast cancer. *BMC Cancer* **14**:841.

Yang J, Yan R, Roy A, Xu D, Poisson J, and Zhang Y (2015) The I-TASSER Suite: protein structure and function prediction. *Nat Methods* **12**:7–8.

Yu W, Chai H, Li Y, Zhao H, Xie X, Zheng H, Wang C, Wang X, Yang G, Cai X, et al. (2012) Increased expression of CYP4Z1 promotes tumor angiogenesis and growth in human breast cancer. *Toxicol Appl Pharmacol* **264**:73–83.

Zheng YM, Baer BR, Kneller MB, Henne KR, Kunze KL, and Rettie AE (2003) Covalent heme binding to CYP4B1 via Glu310 and a carbocation porphyrin intermediate. *Biochemistry* **42**: 4601–4606.

Zöllner A, Dragan CA, Pistorius D, Müller R, Bode HB, Peters FT, Maurer HH, and Bureik M (2009) Human CYP4Z1 catalyzes the in-chain hydroxylation of lauric acid and myristic acid. *Biol Chem* **390**:313–317.

Address correspondence to: Dr. Allan E. Rettie, Department of Medicinal Chemistry, University of Washington, Box 357610, 1959 NE Pacific, Seattle, WA 98195. E-mail: rettie@uw.edu